HHS Public Access

Author manuscript

Trends Dev Biol. Author manuscript; available in PMC 2020 April 03.

Published in final edited form as:

Trends Dev Biol. 2019 ; 12: 1–12.

Targeted deletion of Cyp1b1 in pericytes results in attenuation of retinal neovascularization and trabecular meshwork dysgenesis

Juliana Falero-Perez[1], **Michele C. Larsen**[2], **Leandro B. C. Teixeira**[3,4], **Hao F. Zhang**[5], **Volkhard Lindner**[6], **Christine M. Sorenson**[4,7], **Colin R. Jefcoate**[2], **Nader Sheibani**[1,4,8,*]

[1]Departments of Ophthalmology and Visual Sciences, University of Wisconsin School of Medicine and Public Health, Madison, WI, USA

[2]Department of Cell and Regenerative Biology, University of Wisconsin School of Medicine and Public Health, Madison, WI, USA

[3]Department of Pathological Sciences, School of Veterinary Medicine, Madison, WI, USA

[4]McPherson Eye Research Institute, University of Wisconsin School of Medicine and Public Health, Madison, WI, USA

[5]Department of Biomedical Engineering, Northwestern University, Evanston, IL, USA

[6]Center for Molecular Medicine, Maine Medical Center Research Institute, Scarborough, ME, USA

[7]Department of Pediatrics, University of Wisconsin School of Medicine and Public Health, Madison, WI USA

[8]Department of Biomedical Engineering, University of Wisconsin School of Medicine and Public Health, Madison, WI, USA.

Abstract

Mutations in cytochrome P450 1B1 (CYP1B1) gene are reported in patients with primary congenital glaucoma. *Cyp1b1*-deficient (*Cyp1b1*−/−) mice show dysgenesis of the trabecular meshwork (TM) tissue and attenuation of retinal neovascularization during oxygen-induced ischemic retinopathy (OIR). Although retinal vascular cells, including endothelial cells (EC), pericytes (PC), astrocytes (AC), and TM endothelial cells express CYP1B1, the cell autonomous contribution of CYP1B1 to attenuation of retinal neovascularization and TM tissue dysgenesis remains unknown. Here we determined the impact lack of CYP1B1 expression in EC, PC or AC has on retinal neovascularization and TM tissue integrity. We generated *Cyp1b1*-transgenic mice with vascular cell-specific targeted Cre^{+}-deletion in EC ($Cyp1b1^{EC}$), in PC ($Cyp1b1^{PC}$) and in AC ($Cyp1b1^{AC}$). Pathologic retinal neovascularization during OIR was evaluated by collagen IV staining of retinal wholemounts. Structural morphology of TM tissue was examined by transmission electron microscopy (TEM). The assessment of retinal neovascularization indicated a significant decrease in retinal neovascular tufts only in $Cyp1b1^{PC}$ mice compared with control

*Corresponding author: nsheibanikar@wisc.edu.

CONFLICT OF INTEREST STATEMENT

None.

mice. TEM evaluation demonstrated *Cyp1b1*^{PC} mice also exhibited a defect in TM tissue morphology and integrity similar to that reported in *Cyp1b1*−/− mice. Thus, Cyp1b1 expression in PC plays a significant role in retinal neovascularization and the integrity of TM tissue.

Keywords

cytochrome P450; angiogenesis; endothelial cells; trabecular meshwork cells; oxidative stress

1. Introduction

Cytochrome P450 1B1 (CYP1B1) belongs to the superfamily of proteins that are heme-containing monooxygenases [1]. Although the majority of cytochrome P450s are located in the liver and have important roles in the metabolism of xenobiotics, toxic chemicals and endogenous substrates, recent genetic studies have identified important roles for these molecules in tissue development and function [2]. Mutations in *Cyp1b1* contribute to vascular dysfunctions and glaucoma [1, 3]. CYP1B1 was originally characterized from mouse embryo mesenchymal progenitor cells [4] and has subsequently been examined in other mesenchymal cell types [5-7], including pericytes (PC) [8], neural crest cells [9] and astrocytes (AC) [10]. Exon 3 *Cyp1b1* disruption (*Cyp1b1*−/− mice) [11] established Cyp1b1 participation in obesity through effects on growth hormone and leptin signaling derived from the hypothalamus [12]. Cyp1b1 plays a role in protecting perivascular niche lymphopoiesis [13]. Cyp1b1 deficiency also demonstrates functional vascular roles in the blood brain barrier [14-16]. Thus, Cyp1b1 null mutations can affect various cellular functions and tissue integrity.

Glaucoma is the second leading cause of vision loss in the adult human population [17]. It represents a diverse group of intraocular pressure (IOP)-dependent neurodegenerative disorders that result in loss of normal function and integrity of the retinal neurons and ultimately vision loss [18, 19]. Intraocular pressure is the only proven treatable risk factor for glaucoma. Abnormalities in the aqueous humor drainage pathway are the main cause of elevated IOP [20]. Although less prevalent than the adult forms, primary congenital glaucoma (PCG) causes a devastating loss of vision in children. The pathogenesis of this disease is associated with developmental defects of the conventional outflow pathway, including the trabecular meshwork (TM) and Schlemm’s canal (SC) [21]. However, the underlying mechanisms are not well understood.

We previously established a role for Cyp1b1 in TM cell function, which explained why global loss of Cyp1b1 results in congenital glaucoma [2]. CYP1B1 deficiency in mice resulted in abnormal development and function of the tissues involved in the conventional outflow pathway [3, 22, 23]. We also showed expression of Cyp1b1 is essential for ischemia-mediated retinal neovascularization, and its absence resulted in increased oxidative stress in vascular cells and attenuation of their proangiogenic activities. All these changes were reversed by administration of the antioxidant, N-acetylcysteine [8, 24]. These studies led to the conclusion that Cyp1b1 plays a functional role in maintaining cellular redox homoeostasis.

Trabecular meshwork endothelial cells (EC) are the primary cell type that occupy and form the conventional outflow pathway responsible for the maintenance of homeostatic IOP. *In vitro* studies of human TM cells showed that these neural crest-derived cells display the characteristic features of several different cell types, including vascular endothelial cells and pericytes (PC) [25]. We previously showed that Cyp1b1 is constitutively expressed in vascular EC [24], astrocytes (AC) [26], and PC [8] from vascular beds of many tissues, including retina. We also cultured TM cells from *Cyp1b1*+/+ and *Cyp1b1*−/− mice and showed *Cyp1b1*−/− TM cells present increased apoptotic rates and decreased viability under oxidative challenge, and are more adherent to extracellular matrix (ECM) proteins compared with *Cyp1b1*+/+ cells [23]. In mice, we demonstrated that Cyp1b1 deficiency significantly impaired TM cellular function and redox homeostasis. We showed that the expression of oxidative damage markers was increased in TM tissue from *Cyp1b1*−/− mice, promoting its degeneration. This degeneration was rescued by administration of the N-acetylcysteine [23]. However, the cell autonomous contribution of Cyp1b1 expression to retinal neovascularization and TM tissue defects observed in global *Cyp1b1* null mice remains unknown.

To identify the cell type(s) whose Cyp1b1 expression is essential for these diverse processes, we developed an exon 2 *Cyp1b1*$^{flox/flox}$ mouse that provides the means for lineage-selective Cre deletion of Cyp1b1 (mice conditionally lacking Cyp1b1). By breeding these conditional Cyp1b1 mice to cytomegalovirus-Cre (CMV-Cre) mice we have shown that germline deletion of exon 2 provides a functionally equivalent mice to global *Cyp1b1*−/− mice, in which the exon 3 was disrupted, with respect to the complex intervention in obesity suppression [12]. Here using *Cyp1b1*-targeted transgenic mice, we generated lines of mice which specifically lacked Cyp1b1 expression in EC, PC or AC. We next assessed the impact targeted *Cyp1b1*-deletion in vascular cells has on retinal neovascularization and TM tissue dysgenesis.

2. Methods

2.1. Ethics statement

All experiments were carried out in accordance with the Association for Research in Vision and Ophthalmology Statement for the Use of Animals in Ophthalmic and Vision Research and were approved by the Institutional Animal Care and Use Committee of the University of Wisconsin School of Medicine and Public Health (IACUC assurance number D16-00239).

2.2. Animals

The *Cyp1b1*-targeted mice on the C57BL/6J background were generated using standard procedures. Briefly, targeted Cyp1b1tm1a (KOMP) Wtsi Premium ES cells were obtained from the KOMP Repository (UC-Davis). Chimeric mice were generated in the University of Wisconsin Genome Editing and Animal Models Core Facility. Clone G08 was expanded and subsequently microinjected into blastocysts from C57Bl/6J mice. Injected embryos were transferred into pseudo-pregnant recipients, resulting in seven chimeric mice. *Cyp1b1*^{floxneo} progeny were mated with C57BL/6J mice for 5 generations in the University of Wisconsin Biomedical Research Model Services Core Facility. F1

heterozygote progeny were mated with the Rosa26 Flp recombinase-expressing (Jackson Labs, B6.129S4-Gt(ROSA)26Sortm1(FLP1) Dym/RainJ, Stock# 009086) mouse to remove the neomycin selection marker. The resulting heterozygote littermates (*Cyp1b1*$^{flox/+}$) were mated to generate the *Cyp1b1*$^{flox/flox}$ mice (Figure 1A). The floxed mice were further backcrossed for 10 generations. Genotyping for FLP-recombined allele, intact LoxP sites and *Cyp1b1* Cre-recombined alleles were confirmed by genotyping.

The *Cyp1b1*$^{flox/flox}$ homozygous mice were screened using the following primers: Flanked neomycin cassette 5'-TGGCTGCTCATCCTCTTTAC-3' and 5'-TGGGGAAGGACTCTTAATAC-3', generating a 308-bp band for targeted and a 357-bp band for wild-type (Figure 1B). The removal of neomycin cassette was confirmed using 5'-GGAGCCACTTTCCTGAGGTC-3' and 5'-CTGGGCAAGATGCTTAAAAC-3', primers, which generate a 431-bp band for targeted and a 213-bp band for wild-type allele (Figure 1C).

To establish *Cyp1b1*-specific deletion in EC, PC and AC, we crossed floxed Cyp1b1 mice with VE-cadherin-Cre, Tg(Pdgfrb-Cre)^{45Vli} and Gfap-Cre mice. The VE-cadherin-Cre transgenic mouse line (B6.Cg-Tg (Cdh5-cre)7Mlia/J) was obtained from Jackson Laboratory (Bar Harbor, ME; Stock # 006137). The genotyping was accomplished by PCR analysis of genomic DNA extracted from tail biopsies using the following primers: 5'-GCGGTCTGGCAGTAAAAACTATC-3' and 5'-GTGAAACAGCATTGCTGTCACTT-3'. The Gfap-Cre mouse line B6.Cg-Tg (Gfap-Cre) 73.12Mvs/J was obtained from Jackson Laboratory (Stock # 012886). The genotyping was accomplished by PCR analysis of genomic DNA using the following primers: 5'-TCCATAAAGGCCCTGACATC-3' and 5'-TGCGAACCTCATCACTCGT-3'. The Tg (Pdgfrb-Cre)^{45Vli} mouse line has been described previously [27], and was screened using the following primers: 5'-GCATTTCTGGGGATTGCTTA-3' and 5'-CCCGGCAAAACAGGTAGTTA-3'.

We bred mice homozygous for the *Cyp1b1*$^{flox/flox}$ allele with VE-cadherin-Cre, Tg(Pdgfrb-Cre)^{45Vli} or Gfap-Cre mice to obtain heterozygous mice for the allele that expressed VE-cadherin-Cre, Pdgfrb-Cre or Gfap-Cre. These mice were bred, and the progenies screened, as described above, to obtain mice homozygous for the *Cyp1b1*$^{flox/flox}$ allele that also expressed Cre. Mice homozygous for the *Cyp1b1*$^{flox/flox}$ allele that expressed *VE-cadherin*-Cre, *Pdgfrb*-Cre and *Gfap*-Cre are referred to as *Cyp1b1*^{EC}, *Cyp1b1*^{PC} and *Cyp1b1*^{AC}, respectively. These mice were maintained by breeding mice homozygous for the *Cyp1b1*$^{flox/flox}$ allele that were Cre-expressing to mice homozygous for the *Cyp1b1*$^{flox/flox}$ allele and genotyping. *Cyp1b1*$^{flox/flox}$ mice, the background strain of the *Cyp1b1*^{EC}, *Cyp1b1*^{AC} or *Cyp1b1*^{PC} mice were used as controls, and referred to as control unless noted otherwise. The efficiency of targeted Cre-mediated excision, was previously confirmed with mice carrying a conditional tomato allele and *Pdgfrb*-Cre [28], *VE-Cadherin*-Cre [29, 30] or *Gfap*-Cre [28]. In all experiments, both male and female mice were used.

2.3. Oxygen-induced ischemic retinopathy

Oxygen-induced ischemic retinopathy (OIR) was induced in postnatal day 7 (P7) pups by exposing them to hyperoxia (75% ± 0.5% oxygen) in an airtight incubator for 5 days, as previously described [29-32]. Incubator temperature was maintained at 23 ± 2

°C and oxygen level was monitored continuously using a PROOX model 110 oxygen controller (Reming Bioinstruments Co., Redfield, NY). At the end of the 5-day period (P12), animals were gradually introduced to room air over a period of 5-6 hours before they were transferred into their regular housing area. Animals were kept in room air conditions for five days (P17). The degree of neovascularization was assessed in P17 mice as detailed below.

2.4. Immunofluorescence staining of wholemount retinas

Mice eyes were enucleated, fixed in 4% paraformaldehyde briefly (3-5 min), and transferred to 70% methanol to fix for at least 24 h at −20 °C. Retinas were dissected in and then washed with phosphate buffered saline (PBS) three times, for 10 min each. Dissected retinas were then incubated in blocking buffer (50% fetal bovine serum (FBS) and 20% normal goat serum (NGS) in PBS) for 2 h at room temperature (RT). Retinas were incubated with rabbit anti-collagen IV (Millipore, AB756P), diluted 1:500 in PBS containing 20% FCS, and 20% NGS at 4 °C overnight. Retinas were then washed three times with PBS, 10 min each, incubated with the secondary antibody Alexa 594 goat-anti-rabbit (A-11037; ThermoFisher) diluted 1:500 in PBS containing 20% FCS, 20% NGS for 2 h at RT. Retinas were then washed four times with PBS, 10 min each and mounted on the slide with PBS/glycerol (1:1 vol/vol). Retinas were viewed by fluorescence microscopy and images were captured in digital format using EVOS imaging system (AMG, ThermoFisher).

2.5. Quantification of retinal neovascularization and avascular area

Quantification of retinal and vitreous neovascularization during OIR (at P17) was performed using serial histological sections and image analysis, as described previously by others [31, 33] and us [29, 31]. For histology sections, mice eyes were enucleated and fixed in formalin for at least 24 h at room temperature. Eyes were then embedded in paraffin and eight serial sections (40 μm apart, 6 μm thick) were taken from around the optic nerve (four on each side of the optic nerve). The hematoxylin and PAS-stained slides were examined for the presence of neovascular tufts that had grown from the retina into the vitreous, and the average from 8 sections is reported as the mean number of neovascular nuclei per eye.

For image analysis, after wholemount staining and imaging, retinal neovascularization was assessed by semi-automated quantification method (SWIFT_NV) installed on ImageJ software (NIH, Maryland, USA) as developed and described by Stahl *et al.* [33]. During the preparation of digital captured images for these macros, avascular areas were also measured and reported as percentage of vessel-obliterated area relative to the total retina area.

2.6. Transmission electron microscopy and TM morphometric studies

Eyes from 8-week-old mice maintained under normal housing conditions were enucleated and immersion fixed in 2% paraformaldehyde (PFA) and 2.5% glutaraldehyde in 0.1 M PBS (pH 7.4) at 4 °C overnight. The superior and inferior aspects in the eye of each animal were sampled. Eyes were sectioned on the midsagittal vertical plane and processed for routine transmission electron microscopy evaluation. Briefly, the globes were post-fixed in 2% PFA and 2.5% glutaraldehyde at 4 °C and incubated with 1% OsO_4 in PBS for 2 h at room temperature, followed by three 10-min washes with 0.1 M sodium acetate buffer. Tissues were then stained with 2% uranyl acetate in sodium acetate buffer for 1 h at room

temperature, washed in buffer, dehydrated in a graded ethanol series (40% to 100%), and infiltrated with propylene oxide-812 resin (1005 Embed 812; EMS, Fort Washington, PA). The samples were embedded with fresh 100% 812 resin in molds and polymerized in a 60 °C oven for 36 h. One-micron sections were stained with toluidine blue and examined under the light microscope. Ultrathin sections (90 nm) were analyzed by using a Philips 410 transmission electron microscope (Philips Medical System, Andover, MA).

2.7. Statistical analysis

Statistical differences between groups were evaluated with the one-way ANOVA followed by Tukey's multiple comparison test using GraphPad Prism version 5.04 for Windows (GraphPad Software, La Jolla, CA). Statistical differences were confirmed with Bonferroni's comparison of selected pairs of columns and student's unpaired t-test (two-tailed). Data are presented as mean ± standard deviation, and $P < 0.05$ was considered significant.

3. RESULTS

3.1. Attenuation of pathological retinal neovascularization in pericyte-targeted (*Cyp1b1*^{PC}) mice

CYP1B1 is expressed in vascular EC and its expression is upregulated by shear stress [24, 34, 35]. We previously showed expression of CYP1B1 is essential for ischemia-mediated retinal neovascularization and its global absence resulted in increased oxidative stress in vascular EC and attenuation of their proangiogenic activities [24, 35]. We also showed CYP1B1 is expressed in retinal PC and AC [8, 26]. Although CYP1B1 is constitutively expressed by various retinal vascular cells, their cell autonomous contribution to retinal neovascularization defects detected in the global *Cyp1b1*−/− mice remain unknown. Here using vascular cell-specific targeted *Cyp1b1* transgenic mice, we determined the impact of CYP1B1 deficiency in retinal EC, PC, or AC on retinal neovascularization during OIR.

Cyp1b1$^{flox/flox}$ mice were generated using standard procedures as detailed in Figure 1. These mice were then bred with specific transgenic mice with targeted Cre expression to generate the transgenic mice where *Cyp1b1* was deleted in EC (*Cyp1b1*^{EC}), in PC (*Cyp1b1*^{PC}) and in AC (*Cyp1b1*^{AC}). To elucidate the cell autonomous functional role of CYP1B1 expression in the regulation of pathological neovascularization, *Cyp1b1*-targeted transgenic mice were subjected to OIR. The mouse OIR is a highly reproducible model for studying retinal neovascularization [31]. In this model, P7 mice are exposed to 75% oxygen for 5 days, and then returned to room air for 5 days (P17). The exposure of developing retinal vasculature to high oxygen halts growth of additional vessels and promotes loss of existing immature blood vessels. When animals are returned to room air, the retina becomes ischemic and promotes growth of new blood vessels, which grow into the vitreous and are leaky.

Figure 2A shows representative images of wholemount retinas from *Cyp1b1*$^{flox/flox}$, *Cyp1b1*^{EC}, *Cyp1b1*^{PC} and *Cyp1b1*^{AC} mice subjected to OIR stained with anti-Collagen IV (when maximum preretinal neovascularization occurs). A significant decrease in the degree of neovascularization was observed in P17 *Cyp1b1*^{PC} mice compared to *Cyp1b1*$^{flox/flox}$

littermates subjected to OIR. The quantitative assessment of preretinal neovascularization at P17 is shown in Figure 2B. Similar results were observed using hematoxylin/PAS-stained eye sections from P17 mice subjected to OIR. There were fewer retinal vascular cell nuclei detected on the vitreous side of eyes from *Cyp1b1*^{PC} mice compared with *Cyp1b1*^{EC} and *Cyp1b1*^{AC} mice (not shown). Thus, preretinal neovascularization during OIR in *Cyp1b1*^{PC} mice closely resembles the phenotype previously observed in global *Cyp1b1*−/− mice.

3.2. Disruption and loss of extracellular matrix and degenerative cellular changes in *Cyp1b1* transgenic TM tissues

Trabecular meshwork endothelial cells are the primary cell type that occupy and form the conventional outflow pathway, the primary exit route for aqueous humor from the eye. The TM is best known for its role in the regulation of the intraocular pressure [21]. These neural crest-derived cells display expression patterns and behaviors typical of EC, fibroblasts, smooth muscle cells and macrophages [36]. The normal tissue arrangement in *Cyp1b1*+/+ mice provides tensile strength and flexibility of the TM tissue [37]. The TM needs to maintain its physical properties of elasticity, tension, and softness to ensure the physiological outflow facility [38]. *Cyp1b1*−/− albino mice exhibited severe structural abnormalities in the TM tissue, resembling those reported for human PCG patients; yet those observed in pigmented *Cyp1b1*−/− mice were much more modest [3].

Since TM cells exhibit characteristics similar to other vascular cell types such as EC and PC, we investigated the abnormalities of TM tissues in pigmented *Cyp1b1*^{EC} and *Cyp1b1*^{PC} mice by transmission electron microscopy. Although the TM does not contain AC, both cell types share an embryonic neural crest origin [39, 40]. Besides the TM, the optic nerve head (covered by AC) and the lamina cribrosa undergo the most drastic changes in glaucoma [41]. Thus, we also examined the impact of CYP1B1 expression on the TM of *Cyp1b1*^{AC} mice. Figure 3 shows TM tissues collected from 8-week-old *Cyp1b1*$^{flox/flox}$, *Cyp1b1*^{EC}, *Cyp1b1*^{PC}, and *Cyp1b1*^{AC} mice. The TM from *Cyp1b1*$^{flox/flox}$ mice (Figure 3A; top and bottom) normally consisted of multiple trabecular beams composed of a core of collagen fibers interspersed with small amounts of elastic fibers, surrounded by a single layer of flattened TM endothelial cells. Collagen fibers (Figure 3A, bottom left, asterisk) occupied the core of the beams. The TM cells presented normal cell morphology with a regular cell membrane, homogenous cytoplasm, and close contact with the extracellular matrix core (Figure 3A, bottom left, arrow).

In contrast, conditional *Cyp1b1* mutant mice presented a marked disruption of the anterior and posterior TM tissue, characterized by multifocal atrophy of the trabecular beams with accentuation of the intertrabecular spaces. The collagen and elastic fibers on the ECM layer of the trabecular beams were markedly fragmented and irregularly distributed when compared to the control group (Figure 3B-3D; bottom). We observed that eyes from *Cyp1b1*^{PC} mice exhibited robust atrophy of the trabecular beams marked by the increase in the intertrabecular spaces compared to *Cyp1b1*^{EC} and *Cyp1b1*^{AC} mice. The collagen and elastic fiber fragmentation is more apparent in *Cyp1b1*^{PC} (Figure 3C; bottom) and *Cyp1b1*^{EC} mice (Figure 3D, bottom) compared to *Cyp1b1*^{AC} mice. The TM cells covering

the trabecular beams exhibited irregular cytoplasmic processes, irregular cell projections and loss of contact with basement membranes (Figure 3B-3D, top).

There were no abnormalities presented in the Schlemm's canal (SC) or aqueous vessels in *Cyp1b1*^{AC} and *Cyp1b1*^{PC} mice (Figure 4B, 4C; top). Although the SC in *Cyp1b1*^{AC} mice was normal in length, there were fewer EC lining the TM portion of the SC compared with control mice (Figure 5B; top and bottom), and the EC identified presented a flat and elongated cellular profile with no identifiable intracytoplasmic giant vacuoles (a normal feature of healthy SC endothelial cells). *Cyp1b1*^{EC} mice presented a shorter SC, irregular, distorted and tightly packed TM cells (Figure 4D; top and bottom), fewer EC lining the TM portion of the SC and flat elongated SC endothelial cells with no identifiable intracytoplasmic giant vacuoles (Figure 5D; top). Thus, expression and/or activity of CYP1B1 plays a significant role in proper development and maintenance of the integrity of the conventional outflow pathway.

4. Discussion

CYP1B1 is the product of a candidate gene involved in the pathogenesis of PCG, and is directly related to the compromised integrity and function of the conventional outflow pathway. Our previous studies on the vascular and TM endothelial cells from *Cyp1b1*−/− mice established a significant role for CYP1B1 expression in modulation of vascular cells' redox state and TM integrity [8, 22-24]. These studies established an important role for CYP1B1 as a modulator of cellular and tissue redox homeostasis [2]. Here we investigated the impact cell-specific targeted CYP1B1 expression has on retinal neovascularization during OIR and dysgenesis of the TM tissue. Although a decrease in pathological angiogenesis was noted in *Cyp1b1*^{AC}, *Cyp1b1*^{EC} and *Cyp1b1*^{PC} mice, only *Cyp1b1*^{PC} mice showed a significant decrease in neovascularization. This is likely attributed to CYP1B1 expression being most abundant in PC among vascular cells [8], and their similarity to TM cells embryonic origin and vascular characteristics.

Thrombospondin-2 (TSP2) is a member of the TSP gene family of matricellular proteins, and is closely related to TSP1. TSP2, like TSP1, is a potent endogenous inhibitor of angiogenesis [42, 43]. Purified TSP2 protein inhibits capillary EC migration in culture and blocks corneal neovascularization *in vivo* [43]. This is mediated, at least in part, through the ability of TSP2 to antagonize the proangiogenic activity of vascular endothelial growth factor (VEGF) [44, 45]. We previously showed that lack of CYP1B1 expression in EC, PC or AC resulted in a TSP2 up-regulation [8, 24, 26]. Thus, the enhanced production of TSP2 should aid in the inhibition of pathological angiogenesis. This is consistent with the attenuation of retinal neovascularization observed in the *Cyp1b1*−/− mice during OIR and its reversal by administration of N-acetylcysteine and decreased production of TSP2 [24].

The TM cells at the iridocorneal angle are key regulators of intraocular pressure. Studies of cells in culture isolated from the human TM show that they are unique in many ways, displaying features characteristic of several different cell types, including EC and perivascular supporting cells [25]. Our results showed that histological analysis of the CYP1B1 conditional transgenic mice revealed progressive structural TM abnormalities.

These progressive abnormalities resembled those reported in human patients with primary congenital glaucoma [46-48]. Studies by Libby *et al.* showed severe iridocorneal angle abnormalities in albino *Cyp1b1*−/− mice, characterized by absence of SC and TM. They also reported that the lesions on *Cyp1b1*−/− pigmented (129x1/SvJ x B6) mice were less severe, with animals at 13 months of age presenting attenuated endothelium of the SC and reduction of the TM to a singular trabecular beam [3]. Our laboratory presented similar findings using transmission electron microscopy on younger animals, and protection of the TM by administration of N-acetylcysteine [22, 23].

Conditional *Cyp1b1* mutant mice presented abnormalities in ECM, TM endothelial cell morphology, the degeneration and loss of collagen fibers and dysgenesis of the TM tissue. The severity and distribution of the lesions correlated with the postnatal development period of the TM in mice. At birth, the mouse TM is still immature and reaches full maturity at P35 to P42. By P18, the major developmental changes of the TM have occurred, with subsequent maturation involving final enlargement of spaces in the posterior TM [49]. Our data showed major losses in TM collagen fibrils, irregularities in the TM tissue and TM endothelial cells across all *Cyp1b1* conditional mutant mice with some differences.

Cyp1b1^{EC} mice presented a shorter SC, and fewer EC lining the TM portion of the SC. Ainsworth *et al.* reported that a decrease in the EC number with age is closely linked to an age-related reduction in the size of SC [50]. Although the same phenotype was observed in *Cyp1b1*^{AC} mice, this phenotype was not observed in *Cyp1b1*^{PC} mice. This can be further explained by the disruption of basement membrane, which consists of types I and type IV collagens, laminin-511 and the α6 integrin subunit. This particular integrin-laminin interaction provides adhesive support to secure SC cells to their basement membrane [51], which is compromised in the absence of CYP1B1. We also observed that the SC endothelial cells were more reactive in *Cyp1b1*^{EC} mice compared with control littermates. This could be attributed to the increased oxidative stress and compromised ECM production that affect *Cyp1b1*−/− mice. Since TM cells have both EC and PC-like characteristics, such as neutralizing reactive oxygen species, ECM turnover and contractile tone [36], it is not surprising that vascular cell deficiencies in CYP1B1 disturb this balance in the TM tissue.

The TM tissue forms most of the resistance to the outflow in order to maintain a pressure gradient between intraocular and venous pressure within the eye [52]. The maintenance of these mechanical properties relies on the composition of fibrillar collagens, which support the framework of the TM tissue [53]. We previously showed that ECM changes present in the *Cyp1b1*−/− mice TM tissue alters the mechanical properties necessary to properly respond to injury [22]. Abnormalities in collagen and elastic fibers can affect proper TM tissue elasticity and alter the organization of TM endothelial cells, which can affect the proper movement of the trabecular spaces observed in *Cyp1b1*^{AC}, *Cyp1b1*^{PC} and *Cyp1b1*^{EC} mice, likely leading to increased IOP.

Our group has quantified the amounts of collagen fibers occupying these spaces in *Cyp1b1*−/− mice [23], and a similar phenotype was observed in all conditional Cyp1b1 mutant mice. We previously reported that Cyp1b1 modulates the expression of periostin, an ECM protein essential for collagen fibrillogenesis, by suppression of oxidative stress [23]. Results from

our group showed that the suppression of Cyp1b1 activity, and consequentially, periostin expression, caused marked structural abnormalities in the TM tissue ECM composition. Since the proper organization of the TM tissue is essential for maintaining normal aqueous outflow, these abnormalities are likely responsible for the increased IOP noted in these animals. Overall, these results substantiate an important role for CYP1B1 in dictating the mechanical strength and structural integrity of the collagen-containing TM tissue, especially in the *Cyp1b1*^{EC} and *Cyp1b1*^{PC} mice. However, whether specific expression of CYP1B1 in TM cells similarly affects the integrity and function of TM tissue needs further investigation. Unfortunately, there presently is no Cre-transgenic line available to specifically target TM cells.

In summary, our results show significant attenuation of pathological angiogenesis in *Cyp1b1*^{PC} mice. Here we showed ultrastructural abnormalities on the TM of *Cyp1b1*^{AC}, *Cyp1b1*^{PC} and *Cyp1b1*^{EC} mice, which should impair aqueous outflow, especially in *Cyp1b1*^{PC} and *Cyp1b1*^{EC} mice. Thus, CYP1B1 expression in perivascular supporting cells and EC plays a significant role during ischemia-mediated retinal neovascularization and in the integrity of TM through modulation of cellular redox homeostasis. Therefore, a better understanding of the mechanisms through which CYP1B1 modulates cellular redox homeostasis will provide important insight into angle abnormalities and preventive approaches for glaucoma patients with CYP1B1 mutations.

ACKNOWLEDGEMENTS

This work was supported by an unrestricted award from Research to Prevent Blindness to the Department of Ophthalmology and Visual Sciences, Retina Research Foundation, P30 EY016665, P30 CA014520, EPA 83573701, R24 EY022883, and R01 EY026078. CMS is supported by the RRF/Daniel M. Albert Chair and Villas Life Cycle Professorship. NS is a recipient of RPB Stein Innovation Award. JFP is supported byT32 training grant T32 ES007015. MCL and CRJ were supported by NIH grant R01 DK090249.

REFERENCES

1. Zhao Y, Sorenson CM and Sheibani N 2015, J. Ophthalmic. Vis. Res, 10, 60. [PubMed: 26005555]
2. Falero-Perez J, Song YS, Sorenson CM and Sheibani N 2018, Trends Cell Mol. Biol, 13, 27. [PubMed: 30894785]
3. Libby RT, Smith RS, Savinova OV, Zabaleta A, Martin JE, Gonzalez FJ and John SWM 2003, Science (New York, N.Y.), 299, 1578.
4. Savas U, Bhattacharyya KK, Christou M, Alexander DL and Jefcoate CR 1994, J. Biol. Chem, 269, 14905. [PubMed: 8195121]
5. N'Jai AU, Larsen M, Shi L, Jefcoate CR and Czuprynski CJ 2010, Toxicology, 271, 27. [PubMed: 20171256]
6. Larsen MC, N'Jai AU, Alexander DL, Rondelli CM, Forsberg EC, Czuprynski CJ and Jefcoate CR 2016, Pharmacol. Res. Perspect, 4, e00245. [PubMed: 28116098]
7. N'Jai AU, Larsen MC, Bushkofsky JR, Czuprynski CJ and Jefcoate CR 2011, Mol. Pharmacol, 79, 724. [PubMed: 21252291]
8. Palenski TL, Sorenson CM, Jefcoate CR and Sheibani N 2013, Lab. Invest, 93, 646. [PubMed: 23568032]
9. Chambers D, Wilson L, Maden M and Lumsden A 2007, Development, 134, 1369. [PubMed: 17329364]
10. Filbrandt CR, Wu Z, Zlokovic B, Opanashuk L and Gasiewicz TA 2004, Neurotoxicology, 25, 605. [PubMed: 15183014]

11. Buters JT, Sakai S, Richter T, Pineau T, Alexander DL, Savas U, Doehmer J, Ward JM, Jefcoate CR and Gonzalez FJ 1999, Proc. Natl. Acad. Sci. USA, 96, 1977. [PubMed: 10051580]
12. Larsen MC, Bushkofsky JR, Gorman T, Adhami V, Mukhtar H, Wang S, Reeder SB, Sheibani N and Jefcoate CR 2015, Arch. Biochem. Biophys, 571, 21. [PubMed: 25703193]
13. Rondelli CM, Larsen MC, N'Jai A, Czuprynski CJ and Jefcoate CR 2016, Stem Cells Int., 6, 1753491.
14. Pingili AK, Thirunavukkarasu S, Kara M, Brand DD, Katsurada A, Majid DS, Navar LG, Gonzalez FJ and Malik KU 2016, Hypertension, 67, 916. [PubMed: 26928804]
15. White K, Johansen AK, Nilsen M, Ciuclan L, Wallace E, Paton L, Campbell A, Morecroft I, Loughlin L, McClure JD, Thomas M, Mari KM, and Maclean MR 2012, Circulation, 126, 1087. [PubMed: 22859684]
16. Ziegler N, Awwad K, Fisslthaler B, Reis M, Devraj K, Corada M, Minardi SP, Dejana E, Plate KH, Fleming I, and Liebner S 2016, J. Neurosci, 36, 8921. [PubMed: 27559173]
17. Quigley HA and Broman AT 2006, Br. J. Ophthalmol, 90, 262. [PubMed: 16488940]
18. Jonas JB, Aung T, Bourne RR, Bron AM, Ritch R and Panda-Jonas S 2017, Glaucoma Lancet, 390, 2183. [PubMed: 28577860]
19. Nuzzi R and Tridico F 2017, Front. Neurosci, 11, 494. [PubMed: 28928631]
20. Liu KC, Fleischman D, Lee AG, Killer HE, Chen JJ and Bhatti MT 2020, Surv. Ophthalmol, 65, 48. [PubMed: 31449832]
21. Tamm ER 2009, Exp. Eye Res, 88, 648. [PubMed: 19239914]
22. Teixeira LBC, Zhao Y, Dubielzig RR, Sorenson CM and Sheibani N 2015, Vet. Pathol, 52, 397. [PubMed: 24879660]
23. Zhao Y, Wang S, Sorenson CM, Teixeira L, Dubielzig RR, Peters DM, Conway SJ, Jefcoate CR and Sheibani N 2013, Mol. Cell. Biol, 33, 4225. [PubMed: 23979599]
24. Tang Y, Scheef EA, Wang S, Sorenson CM, Marcus CB, Jefcoate CR and Sheibani N 2009, Blood, 113, 744. [PubMed: 19005183]
25. Tripathi RC and Tripathi BJ 1982, Exp. Eye Res, 35, 611. [PubMed: 6185354]
26. Falero-Perez J, Sorenson CM and Sheibani N 2019, Am. J. Physiol. Cell Physiol, 316, C767P.
27. Cuttler AS, LeClair RJ, Stohn JP, Wang Q, Sorenson CM, Liaw L and Lindner V 2011, Genesis, 49, 673. [PubMed: 21557454]
28. Zaitoun IS, Wintheiser CM, Jamali N, Wang S, Suscha A, Darjatmoko SR, Schleck K, Hanna BA, Lindner V, Sheibani N and Sorenson CM 2019, Sci. Rep, 9, 9700. [PubMed: 31273232]
29. Wang S, Zaitoun IS, Johnson RP, Jamali N, Gurel Z, Wintheiser CM, Strasser A, Lindner V, Sheibani N and Sorenson CM 2017, PLoS One, 12, e0178198. [PubMed: 28552963]
30. Zaitoun IS, Johnson RP, Jamali N, Almomani R, Wang S, Sheibani N and Sorenson CM 2015, PLoS One, 10, e0139994. [PubMed: 26444547]
31. Smith LE, Wesolowski E, McLellan A, Kostyk SK, D'Amato R, Sullivan R and D'Amore PA 1994, Invest. Ophthalmol. Vis. Sci, 35, 101. [PubMed: 7507904]
32. Wang S, Sorenson CM and Sheibani N 2005, Dev. Biol, 279, 205. [PubMed: 15708569]
33. Stahl A, Connor KM, Sapieha P, Willett KL, Krah NM, Dennison RJ, Chen J, Guerin KI and Smith LEH 2009, Angiogenesis, 12, 297. [PubMed: 19757106]
34. Conway DE, Sakurai Y, Weiss D, Vega JD, Taylor WR, Jo H, Eskin SG, Marcus CB and McIntire LV 2009, Cardiovasc. Res, 81, 669. [PubMed: 19126602]
35. Tang Y, Scheef EA, Gurel Z, Sorenson CM, Jefcoate CR and Sheibani N 2010, Am. J. Physiol. Cell Physiol, 298, C665. [PubMed: 20032512]
36. Stamer WD and Clark AF 2017, Exp. Eye Res, 158, 112. [PubMed: 27443500]
37. Gabelt BT and Kaufman PL 2005, Prog. Retin. Eye Res, 24, 612. [PubMed: 15919228]
38. Borras T and Comes N 2009, Exp. Eye Res, 88, 738. [PubMed: 19084518]
39. Tripathi BJ and Tripathi RC 1989, Am. J. Ophthalmol, 107, 583. [PubMed: 2729407]
40. Tao CQ and Zhang X 2014, Developmental Dynamics, 243, 1501. [PubMed: 25236977]
41. Varela HJ and Hernandez MR 1997, J. Glaucoma, 6, 303. [PubMed: 9327349]
42. Lawler J 2000, Curr. Opin. Cell Biol, 12, 634. [PubMed: 10978901]

43. Bornstein P 2009, J. Cell Communic. Signaling, 3, 189.
44. Volpert OV, Tolsma SS, Pellerin S, Feige JJ, Chen H, Mosher DF and Bouck N 1995, Biochem. Biophys. Res. Commun, 217, 326. [PubMed: 8526929]
45. Lawler PR and Lawler J 2012, Cold Spring Harb. Perspect. Med, 2, a006627. [PubMed: 22553494]
46. Maumenee AE 1959, Am. J. Ophthalmol, 47, 827. [PubMed: 13661280]
47. Tawara A and Inomata H 1981, Am. J. Ophthalmol, 92, 508. [PubMed: 7294114]
48. Yan X, Li M, Chen Z, Zhu Y, Song Y and Zhang H 2016, PLoS One, 11, e0145824. [PubMed: 26726880]
49. Smith RS, Zabaleta A, Savinova OV, and John SW 2001, BMC Develop. Biol, 1, 3.
50. Ainsworth JR and Lee WR 1990, Invest. Ophthalmol. Vis. Sci, 31, 745. [PubMed: 2186010]
51. VanderWyst SS, Perkumas KM, Read AT, Overby DR and Stamer WD 2011, Mol. Vis, 17, 199. [PubMed: 21264055]
52. Lutjen-Drecoll E 1999, Prog. Retin. Eye Res, 18, 91. [PubMed: 9920500]
53. Aihara M, Lindsey JD and Weinreb RN 2003, Invest. Ophthalmol. Vis. Sci, 44, 1581. [PubMed: 12657595]

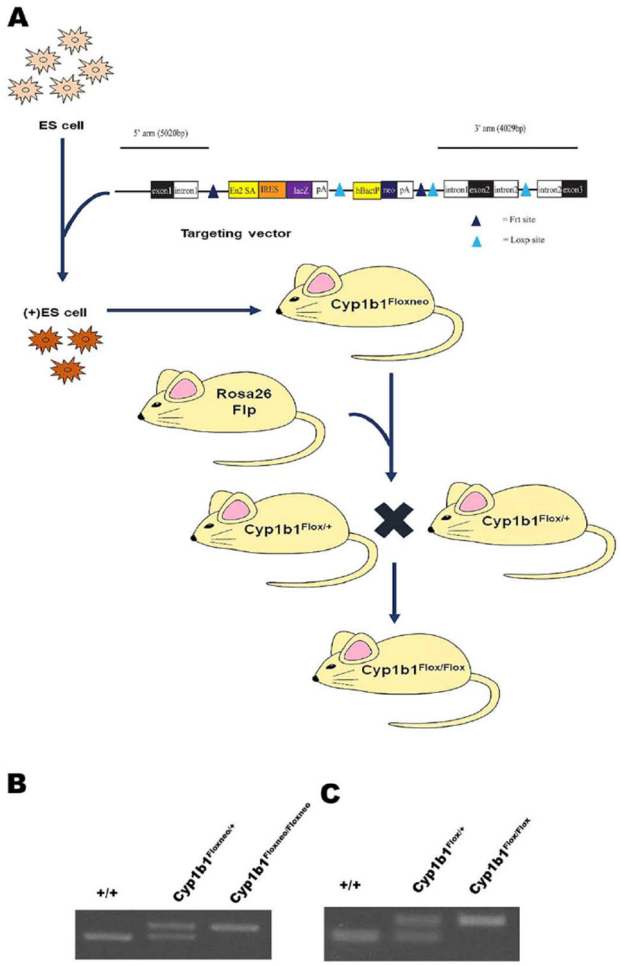

Figure 1.

Generation of the *Cyp1b1* floxed alleles. **A:** Strategy for gene targeting of embryonic stem cells and generation of *Cyp1b1* floxed allele. PCR genotyping analysis of tail DNA samples from *Cyp1b1* floxed mice. **B:** Genotyping for wild type (+/+), $Cyp1b1^{floxneo}$ heterozygous and homozygous alleles. The 308-bp and 357-bp amplified bands were generated from wild-type (+/+), and $Cyp1b1^{floxneo}$ alleles, respectively. **C:** Genotyping for *Cyp1b1*+/+, $Cyp1b1^{flox}$ heterozygous and homozygous alleles. The 431-bp and 213-bp amplified bands were generated from wild type (+/+), and $Cyp1b1^{flox}$ alleles, respectively.

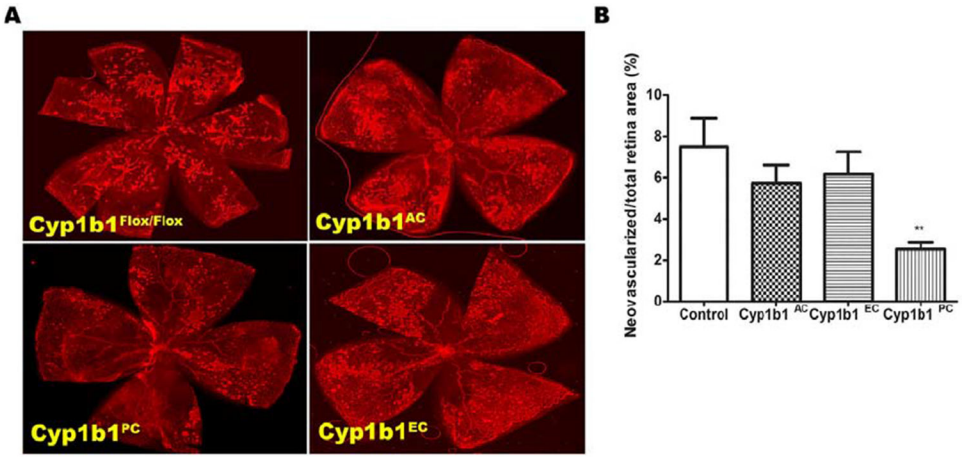

Figure 2.

Attenuation of retinal neovascularization in *Cyp1b1*^{PC} mice. Cyp1b1 conditional transgenic mice were exposed to a cycle of hyperoxia and room air (OIR). **A:** The collagen IV–stained wholemount retinas prepared from P17 *Cyp1b1*$^{flox/folx}$, *Cyp1b1*^{EC}, *Cyp1b1*^{PC} and *Cyp1b1*^{AC} mice are shown (x20). **B:** Quantitative assessment of the neovascularization of all cell-specific *Cyp1b1* conditional transgenic mice. (**$P < 0.005$; $n \geq 6$). Scale bar = 200 μm.

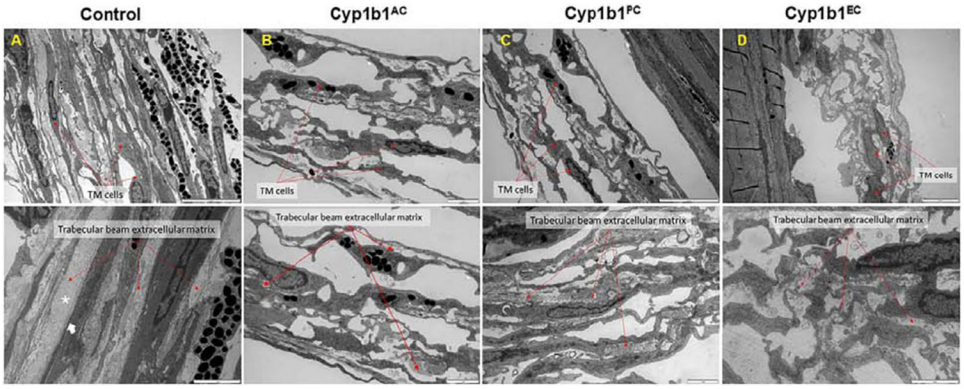

Figure 3.

Trabecular meshwork transmission electron microscopy ultrastructural examination. Tissues collected from 8-week-old *Cyp1b1*$^{flox/flox}$, *Cyp1b1*^{EC}, *Cyp1b1*^{PC} and *Cyp1b1*^{AC} mice. **A:** Normal trabecular meshwork arranged in multiple trabecular beams composed of an extracellular matrix core of collagen and elastic fibers (bottom, asterisk) surrounded by trabecular cells (arrows). **B-D:** Irregular trabecular beams with increased fragmentation of the collagen fibers (arrows, bottom panel) and irregular and reactive trabecular cells (arrows, top panel). Top row scale bar = 5 μm, 2 μm, 5 μm and 5 μm, respectively. Bottom row scale bar = 2 μm.

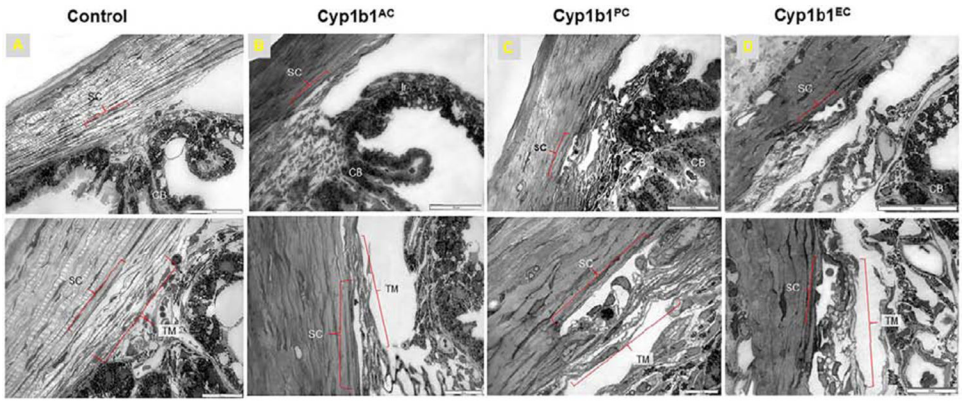

Figure 4.

Trabecular meshwork and Schlemm's canal transmission electron microscopy ultrastructural examination. Tissues from 8-week-old *Cyp1b1*$^{flox/flox}$, *Cyp1b1*^{EC}, *Cyp1b1*^{PC} and *Cyp1b1*^{AC} mice were prepared for TEM studies as described in the 'Methods' section. **A:** Normal morphology for the Schlemm's canal (SC) and TM tissues in the *Cyp1b1*$^{flox/flox}$ mice, top and bottom panel, respectively. **B-C:** Normal Schlemm's canal is observed in *Cyp1b1*^{AC} and *Cyp1b1*^{PC} mice, respectively (top panel). Note, fewer EC (TM) were observed in *Cyp1b1*^{AC} mice (Bottom panel). **D:** Shorter Schlemm's canal was observed in *Cyp1b1*^{EC} mice. Top row (A-D) scale bar = 50 μm. Bottom row (A-D) scale bar = 20 μm, 20 μm, 10 μm and 20 μm, respectively.

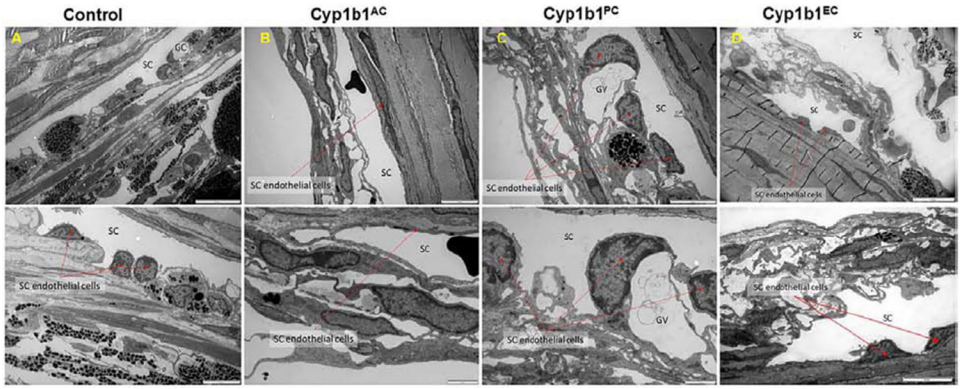

Figure 5.

Transmission electron microscopy ultrastructural examination of Schlemm's canal (SC) endothelial cells. Tissues from 8-week-old *Cyp1b1*$^{flox/flox}$, *Cyp1b1*^{EC}, *Cyp1b1*^{PC} and *Cyp1b1*^{AC} mice were prepared as detailed in the 'Methods' section. **A:** The number of EC in the SC was normal, and typical intracytoplasmic giant vacuoles (GV), a normal feature of these cells, were observed. **B:** Fewer EC were observed in the SC of *Cyp1b1*^{AC} mice and the EC identified presented a flat and elongated profile without intracytoplasmic giant vacuoles. **C:** No changes in SC endothelial cell number and morphology were observed in *Cyp1b1*^{PC} mice. **D:** Fewer SC endothelial cells were observed in *Cyp1b1*^{EC} mice and the EC identified also lacked intracytoplasmic giant vacuoles and presented a flat and elongated profile. Top row (A-D) scale bar = 10 μm, 5 μm, 5 μm and 10 μm, respectively. Bottom row (A-D) scale bar = 5 μm, 2 μm, 2 μm, and 5 μm, respectively.